Journal of Power Sources 565 (2023) 232891

Contents lists available at ScienceDirect

Journal of Power Sources

journal homepage: www.elsevier.com/locate/jpowsour

# Selective chemisorption of polysulfides by porous molecular crystal: Cathode host materials for lean-electrolyte lithium-sulfur cells with high electrochemical stability

Yin-Ju Yen [a,b], Teng-Hao Chen [c], Yao-Ting Wang [b,d], Alexandra Robles [e], Miloš Đerić [e], Ognjen Š. Miljanić [e], Watchareeya Kaveevivitchai [b,d], Sheng-Heng Chung [a,b,*]

[a] Department of Materials Science and Engineering, National Cheng Kung University, No.1 University Road, Tainan City, 70101, Taiwan
[b] Hierarchical Green-Energy Materials Research Center, National Cheng Kung University, No.1 University Road, Tainan City, 70101, Taiwan
[c] School of Pharmacy, National Cheng Kung University, No.1 University Road, Tainan City, 70101, Taiwan
[d] Department of Chemical Engineering, National Cheng Kung University, No.1 University Road, Tainan City, 70101, Taiwan
[e] Department of Chemistry, University of Houston, 3585 Cullen Boulevard #112, Houston, TX, 77204-5003, USA

## HIGHLIGHTS

- The cathode attains high areal/gravimetric capacities and high energy densities.
- A sulfur-loaded cyclobenzoin ester (sulfur-CE) serves as a novel sulfur cathode.
- The sulfur-CE cathode simultaneously attains a high sulfur loading and content.
- The sulfur-CE cathode allows a record-low electrolyte-to-sulfur ratio of 4 μL $mg^{-1}$.
- The sulfur-CE cathode attains a low electrolyte-to-capacity ratio of 4.4 μL mA $h^{-1}$.

## GRAPHICAL ABSTRACT

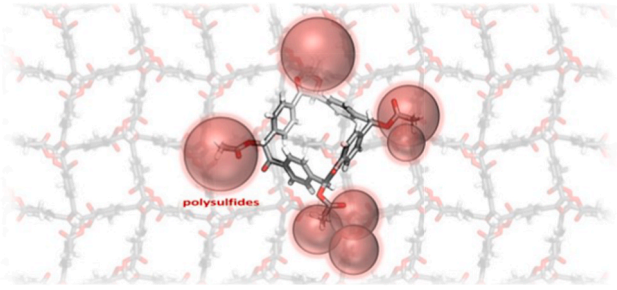


## ARTICLE INFO

*Keywords:*
Porous molecular crystals
Lithium-sulfur batteries
Polysulfides
High-loading cathodes
High sulfur content
Lean-electrolyte cells

## ABSTRACT

The development of high-energy-density lithium-sulfur batteries with porous substrate materials often meets the compromise between the facile accommodation of polysulfides and the fast electrolyte absorption. Porous molecular crystals (PMCs), a new class of organic porous materials assembled by discrete small molecules *via* weak intermolecular interactions, recently show their potential in energy storage. Cyclobenzoin ester (CE), as one of PMCs, features a high abundance of carbonyl groups as a porous molecule. In this study, we utilize the unique adsorption characteristics of CE as an effective sulfur host to design lean-electrolyte lithium-sulfur cells with excellent electrochemical stability. The porosity and polar carbonyl groups of CE provide an excellent chemisorption platform for polysulfides, while also enabling smooth electrolyte penetration. As a result, our sulfur-cyclobenzoin ester (sulfur-CE) energy storage material attains rigorous cell-design parameters with a low electrolyte-to-sulfur ratio (4 μL $mg^{-1}$) and a high sulfur loading/content (4 mg $cm^{-2}$ and 80 wt%), yet exhibits excellent electrochemical characteristics, including an outstanding discharge capacity of 907 mA h $g^{-1}$, cyclability of 200 cycles, and a high rate performance from C/20 to 1C. This research opens a new strategy of selective

* Corresponding author. Department of Materials Science and Engineering, National Cheng Kung University, No.1 University Road, Tainan City, 70101, Taiwan.
*E-mail address:* SHChung@gs.ncku.edu.tw (S.-H. Chung).

https://doi.org/10.1016/j.jpowsour.2023.232891
Received 20 November 2022; Received in revised form 27 January 2023; Accepted 23 February 2023
Available online 3 March 2023

chemisorption for simultaneously optimizing lean-electrolyte lithium-sulfur cells with both high active-material loadings and high cell stability.

## 1. Introduction

Lithium-sulfur batteries are promising energy-storage technologies owing to the high theoretical charge-storage capacity (1675 mA h $g^{-1}$), high theoretical energy density (2600 W h $kg^{-1}$), and low material costs of sulfur [1–3]. In the redox reaction of a lithium-sulfur electrochemical cell, solid-phase sulfur is reduced to long-chain ($6 \leq n \leq 8$) and short-chain ($2 \leq n \leq 6$) liquid-phase polysulfides ($Li_2S_n$), which are reduced to solid-phase lithium sulfide at the end of the discharge process [2]. To promote the practical application of lithium-sulfur electrochemical cells, cathodes must be designed such that the utilization of solid-phase active materials is enhanced, and the diffusion of liquid-phase active-material is inhibited [1–4]. To this end, cathode materials have been optimized to develop various frameworks, such as polysulfides with high reaction activities [3], sulfurated poly (acrylonitrile) with a polymetric polysulfide matrix [5], and organosulfur compounds with novel polymer structures for hosting polysulfides [6]. Moreover, innovative cathode fabrication methods, such as melt-diffusion, ball milling, and dissolution-crystallization [7], have been used to enhance the utilization of active materials. These materials and techniques can be used to develop sulfur cathodes with large sulfur contents in the lean-electrolyte condition, which can be applied to obtain lithium-sulfur cells with high energy densities.

However, the insulating nature of sulfur still limits the development of high-loading sulfur cathodes with sufficient sulfur content, and most existing cathodes have low sulfur loadings (<2 mg $cm^{-2}$) and low sulfur contents (<60 wt%) [8–10]. To address these problems, porous substrates with various functions have emerged as effective sulfur hosts that can prevent the rapid loss of large amounts of polysulfides, especially at increased sulfur loadings. These porous substrates include carbon materials [11,12], metal–organic frameworks [13,14], porous organic polymers [15,16], and covalent organic frameworks [17,18]. Although these porous materials can accommodate polysulfides, they typically suffer from rapid electrolyte absorption, such that high electrolyte-to-sulfur ratios must be implemented to maintain the electrochemical stability of lithium-sulfur cells [1,4,19,20]. To overcome this limitation, it is necessary to develop a high-loading sulfur cathode in a lean-electrolyte cell featuring a long cycle life and a high electrochemical efficiency.

Organic host materials are lightweight, which aids the achievement of high sulfur loadings, and metal-free, which is desirable for sustainable processing and recycling. Porous molecular crystals (PMCs) are a new class of crystalline organic porous materials assembled from discrete small molecules linked *via* weak intermolecular interactions—[π···π] stacking, hydrogen bonds, or [C–H···π] interactions—into ordered frameworks [21–23]. Their solution processability is elusive in polymeric solid host materials, and owing to their adjustable structural properties, PMCs can be used in gas adsorption and separation, molecular recognition, and biomedical applications [24,25]. Moreover, PMCs have recently been applied for energy storage. For example, extrinsically porous hydrogen-bonded organic frameworks have been applied as cathodic materials in lithium-ion batteries [26] and intrinsically porous organic cages have been applied as separators in lithium-sulfur batteries [27]. In these cases, electrochemical performance is enhanced by the formation of ion transport channels and selective ion transport enabled by intermolecular interactions.

In this study, a high-loading sulfur cathode is integrated with a lean-electrolyte cell by using a cathodic substrate based on macrocyclic PMCs assembled by the close-packing of intrinsically porous cyclotetrabenzoin acetate molecules (Fig. 1). Cyclotetrabenzoin acetate is a cyclobenzoin ester and so is denoted as "CE" in the following text. CE exhibits high affinity toward $CO_2$, which enables energy-efficient $CO_2/N_2$, $CO_2/CH_4$, and $CO_2/CO$ separations [25,28]. To develop an energy storage material (sulfur–CE), we load the porous framework of CE with a large amount of sulfur using a simple sulfur-melting process. The abundant carbonyl groups in the molecular structure of CE provide effective chemisorption channels for trapping the polysulfides formed in the electrochemical reactions. Moreover, sulfur–CE exhibits limited absorption capability as it is a nonporous molecule toward ether-based electrolytes [29–31]. With the unique selective adsorption within CE, the sulfur–CE cathode achieves a high sulfur loading and content of 4 mg $cm^{-2}$ and 80 wt%, respectively, and enables the resulting lean-electrolyte cell to exhibit a low electrolyte-to-sulfur ratio (just 4 μL $mg^{-1}$), a long cycle life (200 cycles), and high rate capability (C/20–1C).

## 2. Material and methods

### 2.1. Synthesis of CE and the sulfur-CE energy storage material

Cyclotetrabenzoin acetate (Fig. 1) can be synthesized in two steps on a gram scale, followed by solvent evaporation to afford crystalline compound [32]. The sulfur-CE energy storage material was prepared using a sulfur-melting method. First, sulfur powder (Alfa Aesar, 99.5% precipitated) was uniformly mixed with CE at a weight ratio of 80:20 using a mortar and a pestle, and then heated at 155 °C for 6 h to obtain the sulfur-CE product with a high sulfur content of 80 wt%. We then stirred the sulfur-CE in the electrolyte to form a paste and then drop-cast

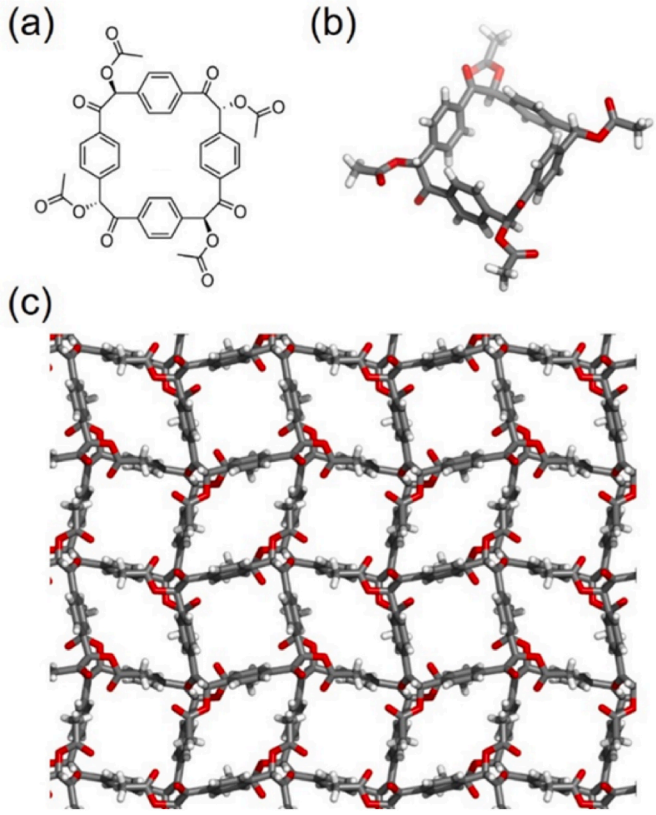


**Fig. 1.** Cyclotetrabenzoin acetate's (a) chemical structure, (b) single crystal structure, and (c) the crystal packing diagram. Element colors: C—gray, O—red, H—white. (For interpretation of the references to color in this figure legend, the reader is referred to the Web version of this article.)

the material on a commercial current collector to form the sulfur-CE composite cathode, which featured a constant high sulfur loading of 4 mg $cm^{-2}$ and a high sulfur content of 80 wt%. A lithium-metal counter/reference electrode was coupled with the sulfur-CE composite cathode, in which a polymeric separator was added to fabricate the lean-electrolyte lithium-sulfur cell with a low electrolyte-to-sulfur ratio of 4 μL $mg^{-1}$, and 10, 8, and 6 μL $mg^{-1}$ (see the Supporting Information). The electrolyte-to-sulfur ratio was calculated based on the total volume of electrolyte added in the electrochemical cells and the total sulfur mass in the same cell. The electrolyte was prepared with 1.85 M lithium bis (trifluoromethanesulfonyl)imide (LiTFSI, Sigma Aldrich, 99.95% trace metals basis) and 0.2 M lithium nitrate ($LiNO_3$, Alfa Aesar, 99.98% anhydrous) in a 1,3-dioxolane (DOL, Alfa Aesar, 99.5%)/1,2-dimethoxyethane (DME, Alfa Aesar, 99+%) mixture at a volumetric ratio of 40:55. A reference sulfur cathode was prepared with a paste containing sulfur, conductive carbon black, and polyvinylidene difluoride binder by a weight ratio of 80:10:10 in *N*-methylpyrrolidine. The paste was prepared using the same drop-cast method on the current collector.

### 2.2. Material characterization

The crystalline structure of the synthesized sulfur-CE energy storage material was characterized using an X-ray diffractometer (XRD, Bruker, D8 DISCOVER) with Cu Kα radiation (λ = 1.4506 Å) from 10° to 70°. The surface morphology and elemental distribution were examined using a field-emission scanning electron microscope (FE-SEM, HITACHI, SU8000) equipped with an energy dispersive X-ray spectrometer (EDS, HITACHI, SU8000). The chemical compositions of the CE molecular crystal and sulfur-CE energy storage material were investigated by thermogravimetric analysis (TGA), Raman spectroscopy, and X-ray photoelectron spectroscopy (XPS) analysis. The TGA was conducted using a thermogravimetric analyzer (PerkinElmer, TGA4000) with a ramping rate of 5 °C $min^{-1}$ and a temperature range of 50–600 °C. The Raman analysis was conducted using a micro-Raman system (ULVAC, Jobin Yvon/Labram HR) from 100 to 2000 $cm^{-1}$ at 532 nm excitation wavelength. The XPS analysis was measured using a PHI 5000 VersaProbe and fitted using the CasaXPS software with Voigt functions after a subtraction of a Shirley–type background. The polysulfide adsorption experiment was conducted with 20 mg of CE and sulfur-CE energy storage material in a dilute polysulfide solution, and a static polysulfide adsorption period of one week at room temperature. The absorbance of the resulting solutions was analyzed by the UV–visible spectrometer (HITACHI, U4100) from 200 to 800 $cm^{-1}$. The dilute polysulfide solution containing 3 mM $Li_2S_6$ was synthesized by mixing sulfur and lithium sulfide ($Li_2S$, Alfa Aesar, 99.9% metals basis) with a molar ratio of 5:1 at 70 °C in a mixture of DOL/DME overnight.

### 2.3. Electrochemical test

The electrochemical tests, including electrochemical characteristics and performance of the cell, were all based on the same cell-design parameters with the high sulfur loading of 4 mg $cm^{-2}$ and high sulfur content of 80 wt% in the lean-electrolyte lithium-sulfur cell with the low electrolyte-to-sulfur ratio of 4 μL $mg^{-1}$. The electrode size was fixed as 1 × 1 $cm^2$. Thus, we studied and demonstrated the electrochemical characteristics and performance of the cell at the same analysis condition. Specifically, the galvanostatic discharge/charge analysis was conducted using a programable battery cycler (NEWARE, CT-4008-5V10mA) at room temperature. The cyclability of the sulfur-CE cathode was examined at a cycling rate of C/10 between 1.8 V and 2.8 V for 200 cycles with the reference sulfur cathode as a comparison. The nucleation and dissolution of sulfide were investigated by analyzing the charge and discharge curves obtained in the cyclability measurements at C/10 rate. The rate performance of the sulfur-CE cathode and the reference sulfur cathode was characterized at cycling rates of C/20, C/10, C/5, C/2, and 1C. After cycling at these 5 different rates, the sulfur-CE and reference cathodes were cycled back to the C/10 rate for another 10 cycles for analyzing the reversibility. Each cycling rate was repeated for 10 cycles for evaluating the rate performance. Moreover, the sulfur-CE cathode was analyzed at various cycling rates of C/10, C/7, and C/5 for a long cycle life of 200 cycles to simultaneously demonstrate the cyclability and rate capability. The electrochemical impedance analysis of the fresh and cycled cathodes was measured in a frequency range of 1 MHz–10 mHz, with an AC voltage amplitude of 5 mV at the open circuit voltage (OCV) using a potentiostat (Biologic, SP-150). The analytical impedance results were used to calculate the lithium-ion diffusion coefficient ($D_{Li}^{+}$) at the fresh and cycled state of the cells using Arrhenius equation, $D_{Li^+} = \frac{R^2T^2}{2A^2n^4F^4C^2\sigma^2}$, in which $R$ is the ideal gas constant, $T$ is the absolute temperature, $A$ is the cathode area, $n$ is the number of electrons, $F$ is the Faradaic constant, $C$ is the lithium concentration, and $\sigma$ is the Warburg factor. The cyclic voltammetry (CV) of the sulfur-CE and the reference cathodes was performed with four scanning rates of 0.01, 0.02, 0.03, and 0.04 mV $s^{-1}$, each repeated for 3 cycles. The lithium-ion diffusion coefficient was further considered by calculating the CV data *via* the Randles–Ševčík equation in the case of a constant-voltage redox reaction. The Randles–Ševčík equation is denoted as $i_{peak} = 268,600 \times e^{1.5} \times area \times coefficient_{Li-ion}{}^{0.5} \times concentration_{Li-ion} \times rate^{0.5}$, in which $i_{peak}$ is the peak current, $e$ is the number of electrons, *area* is the cathode area, $coefficient_{Li-ion}$ is the lithium-ion diffusion coefficient, $concentration_{Li-ion}$ is the lithium-ion concentration in the electrolyte, and *rate* is the scanning rate. The symmetric cell with CE as the electrode was prepared with and without 0.2 M $Li_2S_6$ in the electrolyte and analyzed at 5 mV $s^{-1}$ between −1.0 V–1.0 V.

## 3. Results and discussion

### 3.1. Synthesis of the sulfur-CE energy storage material

The chemical structure of the PMC material, cyclotetrabenzoin acetate, is shown in Fig. 1(a) [32]. The structural features of cyclotetrabenzoin acetate are the square micropores (7.1 × 7.1 Å) with four roughly parallel benzene walls and four carbonyl groups (Fig. 1(b)). Two types of 1D channels are observed in the crystal structure of packed cyclotetrabenzoin acetate (Fig. 1(c)): the square one which is intrinsic to the molecule of cyclotetrabenzoin acetate, and the diamond-shaped one from the extrinsic voids between the molecules of cyclotetrabenzoin acetate. The carbonyl groups pointing inward the benzene-walled channels generate a polar environment with π-interactions suitable for the polysulfide adsorption [29,30]; cyclotetrabenzoin acetate is characterized by a Brunauer-Emmett-Teller (BET) surface area of 572 ± 16 $m^2$ $g^{-1}$ and a pore volume of 0.18 $cm^3$ $g^{-1}$. We hypothesize that such CE crystals would make a good cathode substrate for lithium-sulfur batteries due to this unique combination of porosity and polar functional groups that could trap polysulfide species and prevent the loss of active material, while limiting the electrolyte absorption of the CE substrate. To investigate the possibility of selective adsorption, we incorporate sulfur into CE as the sulfur-CE energy storage material with a sulfur loading of 4 mg $cm^{-2}$ and a sulfur content of 80 wt% to demonstrate the porous behavior in hosting the active material. The sulfur-CE cathode is then investigated in a series of lean-electrolyte cells to demonstrate the nonporous behavior in reaching the lowest electrolyte-to-sulfur ratio of 4 μL $mg^{-1}$ (see Experimental Section for details).

We examine the chemical and physical characteristics of the sulfur-CE powder using X-ray diffraction (XRD), Raman spectroscopy, and thermogravimetric analysis (TGA) (Fig. 2). The XRD result in Fig. 2(a) shows that the crystalline structure of our synthesized CE is consistent with previous reports [32]. After the encapsulation of sulfur during the sulfur-melting treatment, the resulting sulfur-CE material shows strong intensity from the diffraction peaks of sulfur (PDF#08–0247), indicating a high amount of CE is composed of discrete small molecules that are tightly packed by weak intermolecular interactions. When the intrinsic

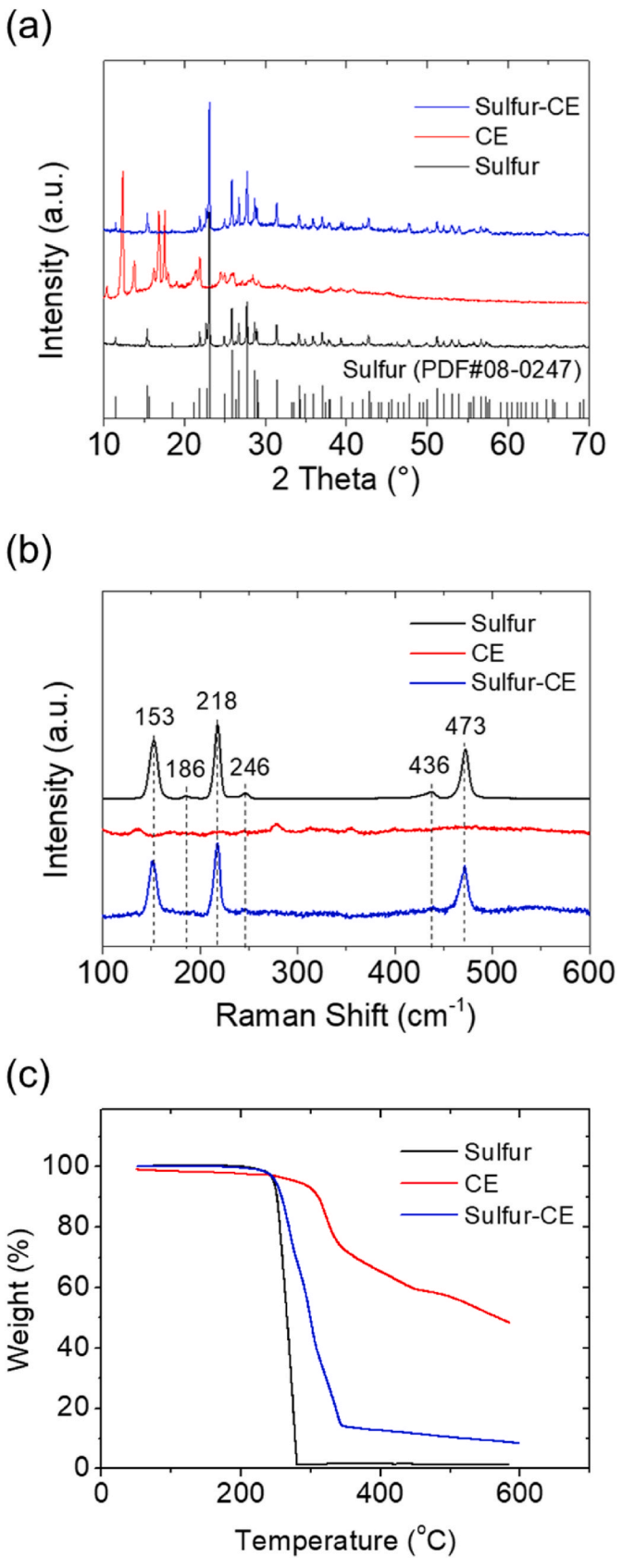


**Fig. 2.** Materials characterization of sulfur, CE, and the sulfur-CE energy storage material: (a) XRD, (b) Raman, and (c) TGA analysis.

pores of the ring molecule itself and the extrinsic gap between CE molecules are occupied by the incorporated sulfur *via* the intermolecular forces, this changes the stacking order of CE and therefore results in the low XRD intensity of CE in the sulfur-CE composite. Thus, the XRD analysis of CE and sulfur with the comparison with sulfur-CE confirms the formation of the sulfur-CE composite that strongly host the sulfur in the framework of CE. The same phenomenon is also observed in the Raman analysis in Fig. 2(b), with strong sulfur peaks at 153, 218, and 473 $cm^{-1}$ detected in the same range for sulfur and the sulfur-CE energy storage material [33,34]. Compared to the Raman spectrum of pure sulfur, the minor peaks at 186, 246, and 436 $cm^{-1}$ of sulfur disappear in the sulfur-CE material. This phenomenon may result from the phase transformation of sulfur from solid to liquid during the sulfur-melting process, in which minor peaks are covered by the major peaks [35]. To further confirm the strong sulfur incorporation, we observe the weight change of sulfur, CE, and sulfur-CE with the temperature by the TGA analysis. In Fig. 2(c), the sulfur-CE energy storage material starts to have a weight loss at a similar temperature of 240 °C as that of pure sulfur. At 280 and 340 °C, pure sulfur and sulfur-CE composite show the weight loss of ~99 wt% and ~86 wt%, respectively. The CE shows a weight loss of 27 wt% at 340 °C. In consideration of the sulfur-CE composite prepared with 20 wt% CE, the TGA data suggest a weight loss of 5–6 wt% in the sulfur-CE composite that might result from CE. This indicates a high content of sulfur approaching 80 wt% in the sulfur-CE material. Based on the results of XRD, Raman, and TGA analyses, we draw a conclusion that the CE molecular crystals could incorporate with sulfur to form the sulfur-CE energy storage material featuring a strong sulfur content.

We then investigate the surface morphology and elemental distribution of the sulfur-CE energy storage material, comparing to pure sulfur and CE (Fig. 3 and S1). The scanning electron microscopy (SEM) and corresponding energy dispersive x-ray spectroscopy (EDS) images in Fig. 3(a) and S1(a)show the pure sulfur as irregular and distinct particles with a strong elemental sulfur signal. Fig. 3(b) and S1(b)show the CE sample, which is composed of clusters with a highly rough surface along with overlapping carbon and oxygen signals that belong to the abundant carbonyl groups constructing the molecular structure [36]. Finally, the sulfur-CE sample shows that the CE clusters feature a slightly muddier surface (Fig. 3(c) and S1(c)). The similarity in the cluster morphology of CE and sulfur-CE as well as the differences of the rough and muddy surfaces suggest that sulfur melts and covers the rough surface of CE during the fabrication process, which is also evidenced by the elemental mapping that shows the presence of sulfur in addition to the carbon and oxygen signals (Fig. 3(c)). As a result, the phase-identification, thermal, morphological, and elemental analyses confirm the successful synthesis of the sulfur-CE energy storage material, which features the CE structure as the matrix that incorporates the trapped sulfur in the porous structure and the functional surface of CE matrix.

### *3.2. Electrochemical analysis and cell performance of the sulfur-CE cathode*

We subsequently analyze the electrochemical and cell performance of the sulfur-CE cathode (Figs. 4 and 5). To ensure practical analytical results, all data are obtained using the same rigorous cell-design parameters, including a high sulfur loading of 4 mg $cm^{-2}$, a high sulfur content of 80 wt%, and a low electrolyte-to-sulfur ratio of 4 μL $mg^{-1}$. These parameters exceed the required parameters in the development of lithium-sulfur technology [2–4,7–9,37]. Moreover, we simultaneously adopt all critical parameters used for developing both a high-loading sulfur cathode and lean-electrolyte lithium-sulfur cell.

We measure the electrochemical impedance spectra of the sulfur-CE cathode and a sulfur-carbon reference cathode before and after cycling for 200 cycles (sulfur-CE cathode) and 50 cycles (reference cathode), which are shown in Fig. 4(a) and (b), respectively. Both cathodes before and after cycling display a semicircle in the higher frequency region that

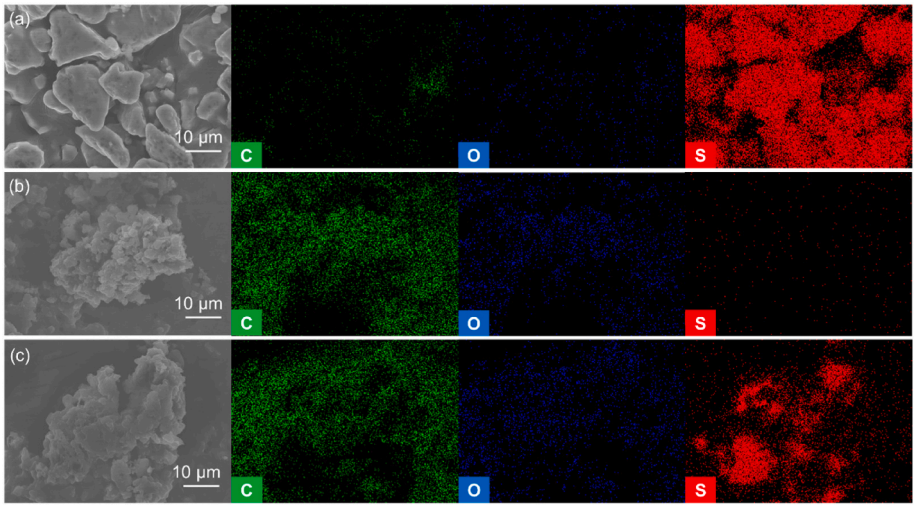


**Fig. 3.** The SEM and corresponding EDS results of (a) sulfur, (b) CE, and (c) the sulfur-CE energy storage material.

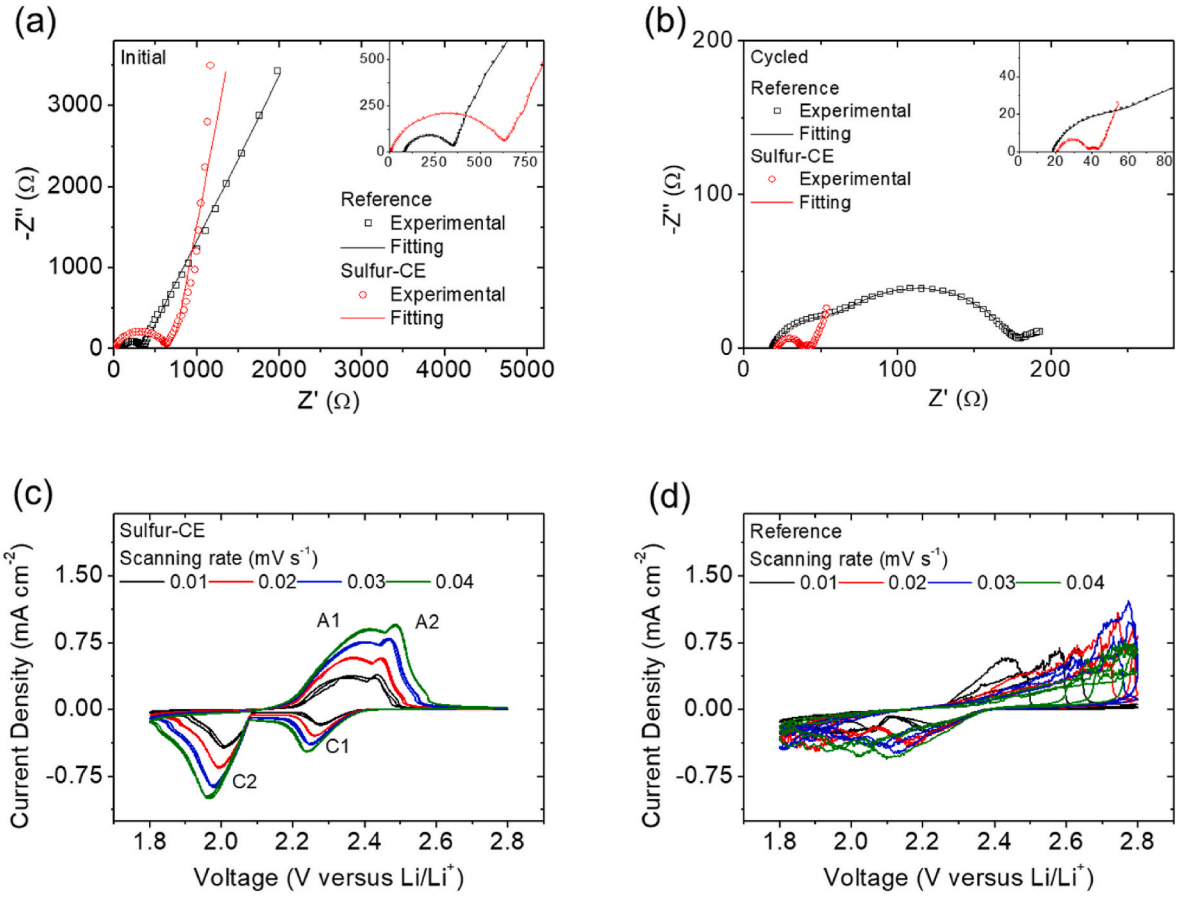


**Fig. 4.** The electrochemical impedance spectra and the fitting results of the sulfur-CE cathode and the reference cathode: (a) before cycling and (b) after cycling for 200 cycles (sulfur-CE cathode) and 50 cycles (reference cathode) at a C/10 rate. The CV scanning results of (c) the sulfur-CE cathode and (d) the reference cathode with scanning rates of 0.01–0.04 mV $s^{-1}$.

corresponds to the charge-transfer resistance. After the cycling test, the second semicircle in the lower frequency region in both the sulfur-CE cathode and reference cathode might be an indication of the passivation-layer resistance. The fitting results and the equivalent Randles circuit of the fresh and cycled cathodes are shown in Table S1 and Fig. S2. The fresh sulfur-CE cathode exhibits a charge-transfer resistance of 546.3 Ω, which we attribute to the use of the low conductive CE as the host material but not the conventional conductive carbon and the use of additional carbon additives. However, the charge-transfer resistance is drastically decreased to 16.6 Ω after cycling for 200 cycles for the sulfur-CE cathode. The decrease in the charge-transfer resistance may be due to the strong polysulfide-trapping capability contributed by the abundant carbonyl groups of the CE substrate, which results in the redistribution and high retention of the dissolved

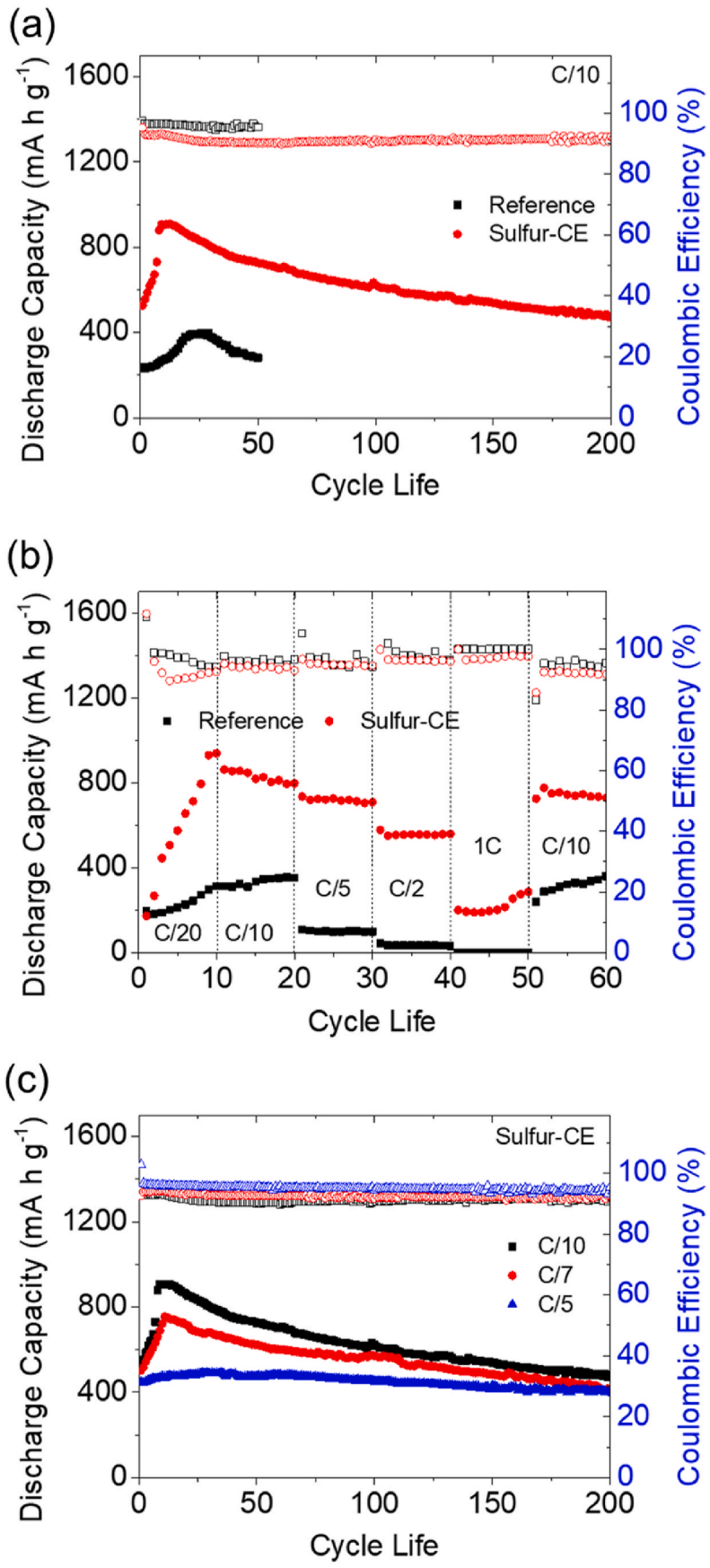


**Fig. 5.** (a) The cyclability of the sulfur-CE and reference cathodes at the C/10 rate. (b) The rate performance of the sulfur-CE and reference cathodes at C/20–1C rates. (c) The cyclability of the sulfur-CE cathode at the C/10, C/7, and C/5 rates.

polysulfides that have strong reaction activity. This improved reaction kinetics also implies the facilitation of the high active-material utilization. After a long-term cycling process of 200 cycles, a passivation layer composed of $Li_2S$ still forms with minor effect on the performance of the sulfur-CE cathode due to the insulating nature of CE. In contrast, despite the fresh reference cathode has a relatively low charge-transfer resistance of 255.8 Ω due to the contribution of the conductive carbon, it suffers a high resistance of 117.0 Ω after cycling for just 50 cycles. The high resistance of the cycled cathode results from the dissolved polysulfides, which diffuse out from the reference cathode's conductive network during each cycle. This process leads to the loss of the active material and causes the continuous deposition of an insulating sulfide covering on the cathode [7–9].

Using this electrochemical impedance analysis, we calculate the lithium-ion diffusion coefficient ($D_{Li}^{+}$) from the diffusion region [38]. From the Arrhenius equation, the Warburg factor (σ) can be obtained by the linear relationship between the real impedance (Z') and the square root of the frequency ω in the low-frequency region, as shown in Figs. S3 (a) and (b). The calculated $D_{Li}{}^{+}$ values of the of sulfur-CE and reference cathodes change from $9.2 \times 10^{-15}$ to $3.7 \times 10^{-11}$ $cm^2$ $s^{-1}$ and from $1.2 \times 10^{-15}$ to $8.9 \times 10^{-12}$ $cm^2$ $s^{-1}$ after cycling, respectively, indicating that the sulfur-CE cathode has better lithium-ion diffusion in the cell and during the cell operation as compared to that obtained from the reference cathode.

Fig. 4(c) showing the cyclic voltammetry (CV) curves of the sulfur-CE cathode makes a summary of the lithium-sulfur electrochemistry in terms of the intrinsic material science and the extrinsic fabrication design. Fig. S4 shows the corresponding CV curves repeated at each scanning rate from 0.01 to 0.04 mV $s^{-1}$. The sulfur-CE cathode forms two cathodic peaks (C1 and C2) and two anodic peaks (A1 and A2) during the redox reaction. Specifically, the redox reaction of the lithium-sulfur cell involves the reduction of the solid-phase sulfur to liquid-phase polysulfides (C1) and solid-phase sulfide (C2), and the reversible oxidation reaction from sulfide to polysulfides (A1) and sulfur (A2) with solid-liquid-solid phase conversion [39]. The sulfur-CE cathode exhibits overlapping CV curves with no shifts of the cathodic and anodic peaks as the scanning number and rate increase, demonstrating its excellent electrochemical stability and reaction kinetics. The improved reaction kinetics and electrochemical stability are further affirmed by a symmetric cell with CE. The cell shows a higher CV current than that of the reference without polysulfides. This confirms that the CE is catalytically active and electrochemical stable in the lithium-sulfur cell environment (Fig. S5). Moreover, with a high sulfur content and loading, the sulfur-CE cathode displays limited polarization and almost no IR drop in the lean-electrolyte cell as the scanning rate increases. Thus, the CV results further confirm the excellent redox reversibility of the sulfur-CE cathode. In contrast, the reference cathode assembled with the same sulfur loading and content fails to complete the reversible electrochemical reactions in the same lean-electrolyte lithium-sulfur cell (Fig. 4 (d) and S6). The high polarization and shifts in the redox peaks indicate the deterioration of the original sluggish electrochemical conversion reaction. As the scanning number and rate increase, the severe peak shift, the disappearance of the redox peaks, and the appearance of strong IR drops indicate the high polarization and difficulty in maintaining normal redox processes in the reference cathode. These trends are consistent with the challenges encountered in the development of high-loading sulfur cathodes (*i.e.*, high polarization) and lean-electrolyte cells (*i.e.*, poor redox reversibility and poor electrochemical stability) [2–8,37], which our sulfur-CE cathode is notably able to avoid.

Based on the CV analysis, we further calculate the lithium-ion diffusion coefficients from the slope of the current to the square root of the scanning rate [39] in Fig. S7 to understand the lithium-ion diffusion during the cell's electrochemical conversions from solid-phase to liquid-phase polysulfides (C1 and the reversible reaction at A2) and from liquid-phase polysulfides to solid-phase sulfides (C2 and the reversible reaction at A1). The lithium-ion diffusion coefficients of C1, C2, A1, and A2 are $4.6 \times 10^{-9}$, $1.7 \times 10^{-8}$, $1.4 \times 10^{-8}$, and $1.8 \times 10^{-8}$ $cm^2$ $s^{-1}$, respectively. These values are consistent with the trend in the results of the impedance analysis, though they are higher values than those of the analytical impedance results since the electrochemical impedance analysis measures a more equilibrium state [40]. However, the reference cathode suffers a deteriorated conversion as the scanning rate increases in the constant-voltage redox reaction, which implies the unsuccessful conversion reaction.

We next demonstrate the cycling performance of the sulfur-CE and reference cathodes in Fig. 5, which we compare at a cycling rate of C/10 (Fig. 5(a)). The sulfur-CE cathode displays a gradual climb in the discharge capacity and reaches a peak charge-storage capacity of 907 mA h $g^{-1}$, attaining an excellent low electrolyte-to-capacity ratio of 4.4 μL mA $h^{-1}$ (that is less than the needed 5- μL mA•$h^{-1}$ and is rarely attained in most research). With the high-loading sulfur cathode design, the sulfur-CE cathode attains superior areal and gravimetric capacity values of 3.6 mA h $cm^{-2}$ and 726 mA h $g^{-1}$, respectively, with the comprehensive consideration of the practical electrode dimensions. The increasing capacity in the first few cycles is due to the redistribution and activation of the active material, which is merited by the abundance of carbonyl groups in CE. The carbonyl groups in CE can effectively adsorb and accommodate the polysulfides. The polysulfides stabilized within the cathode region contribute their strong reaction activity and capacity as well as serve as the catholyte to activate the unreacted insulating solid-phase active materials remaining in the cathode [3,29–31]. In addition, the porous structure in CE does not take up too much electrolyte, allowing the sulfur-CE cathode to operate in lean electrolyte conditions [2,37,39], thus contributing to the excellent cycling performance with a reversible capacity of 470 mA h $g^{-1}$ after 200 cycles. In contrast, using the same fabrication parameters, the reference cathode only attains a low discharge capacity of 397 mA h $g^{-1}$ and a reversible capacity of 281 mA h $g^{-1}$ after 50 cycles. The poor performance of the reference cathode shows that the sulfur-CE cathode design better utilizes the sulfur active material. Besides, CE enables the high-sulfur-loading sulfur-CE cathode to attain superior electrochemical utilization in the lean-electrolyte cell for a long cycle life, outperforming the currently reported lithium-sulfur performance and promoting the feasibility of lithium-sulfur cathode technology (Fig. S8 and Table S2).

The rate performance has proven to be a major challenge for high-loading cathodes, since the high amount of insulating sulfur exacerbates the sluggish conversion reaction as the current density rises [1]. On the other hand, the use of lean-electrolyte cells highlights the challenges of polysulfides and poor lithium-ion transfer in the sulfur cathode chemistry during the high power operation [39]. However, it is necessary to develop an integrated cell system to achieve a high energy density along with a high rate performance [2,8,9,41,42]. We compare the rate performance of the sulfur-CE cathode with the reference sulfur cathode at various cycling rates from a slow C/20 rate to a fast 1C rate. The sulfur-CE cathode achieves high discharge capacity values of 938, 797, 708, 556, and 285 mA h $g^{-1}$ at different cycling rates of C/20, C/10, C/5, C/2, and 1C, respectively. After then returning to the C/10 rate, the cell maintains a high discharge capacity of 775 mA h $g^{-1}$, demonstrating an excellent reversibility of 97% (Fig. 5(b)). However, the reference cathode only displays discharge capacity values of 313, 353, and 98 mA h $g^{-1}$ at C/20, C/10, and C/5, respectively, and soon fails at C/2 and 1C rates due to its deteriorating poor cyclability. The rate performance of the cathodes confirms that the CE substrate helps address the polysulfide diffusion and redeposition as insulating deposits, as well as avoiding the tradeoff between strong polysulfide adsorption and high electrolyte consumption.

We also analyze the long-term cyclability of the sulfur-CE cathode at fast cycling rates in Fig. 5(c). The cells display their peak discharge capacities of 907, 755, and 500 mA h $g^{-1}$ with a high capacity retention of 52%, 55% and 82% after cycling at C/10, C/7, and C/5 rates, respectively, for 200 cycles. The sulfur-CE cathode shows the strong

initial capacity increase at the relatively low cycling rates. This might result from the sufficient time for the active material to redistribute toward the electrochemical favorable positions in the cathode and for the polysulfide catholyte to form and to activate the unreacted solid-phase active materials. The long-term cyclability test of the sulfur-CE cathode at three cycling rates demonstrates that the sulfur-CE cathode can be operated at both slow and fast cycling rates with cycling stability that remains high and features improved capacity retention rate. The high-rate and long-term cyclability analysis reconfirms that the CE substrate is effective at chemically trapping active polysulfides to accelerate the electrochemical reaction of the high-loading sulfur cathode, while it also promotes low electrolyte consumption to maintain the smooth lithium-ion transfer in the lean-electrolyte lithium-sulfur cell.

A summary of the detailed galvanostatic charge/discharge curves of the sulfur-CE and reference cathodes at the constant cycling rates of C/10, C/7, and C/5, and the rate performance from C/20 to 1C rates is shown in Figs. S9–S11. Both cathodes display two typical discharge plateaus, which are assigned to the conversion of sulfur to polysulfides and polysulfides to lithium sulfide, respectively; while two charge plateaus correspond to the reversible sulfide-polysulfide-sulfur conversion [42,43]. No additional electrochemical charge/discharge reactions could be found; thus, we reconfirm that the redox reactions are mainly contributed by sulfur with no side reactions. In the long-term cyclability test, as shown in Fig. S9, the sulfur-CE cathode shows overlapping charge and discharge plateaus, with a small polarization and a minor loss of the discharge capacity, while a large polarization is observed in the reference cathode (Fig. S9(d)). Moreover, Figs. S10(a) and (b) explore the conversion of the active material involving the nucleation of sulfide and the dissolution of sulfide, respectively. In both active-material conversion processes, the sulfur-CE cathode shows a decrease trend in the low polarization. However, the reference cathode encounters high polarization that further increases during cell cycling. This confirms the sulfur-CE cathode's improved redox kinetics [3,44,45]. Additionally, in Fig. S11, the polarization in the reference cathode becomes worse as the scanning rate increases, indicating the difficulty in completing a normal redox reaction when developing lithium-sulfur technology toward lean-electrolyte cells with a high-loading sulfur cathode. However, the high-loading sulfur-CE cathode might offer a possible solution.

### 3.3. Selective adsorption of CE in the lithium-sulfur electrochemistry

To better understand the possible chemisorption effect by the carbonyl groups on CE, we compare the solution color in the polysulfide adsorption experiment with the addition of CE and the sulfur-CE energy storage material in a dilute polysulfide solution. Fig. 6(a) shows the as-synthesized polysulfide blank solution, which features a light-yellow color. However, after dispersing the CE and sulfur-CE powder in the solution, the color turns brown and dark brown, respectively. The change in the color difference compared to the blank polysulfide solution may be contributed to the good dispersion of CE in the solution, and increased sulfur concentration by adding sulfur-CE powder. After resting for one week, as shown in Fig. 6(b), the color of the blank solution is unchanged, while the samples containing CE and sulfur-CE have turned lighter. The obvious color change suggests that the abundant carbonyl groups in CE can chemically adsorb a high amount of polysulfides, even when the material has been pre-loaded with sulfur as in the case of the sulfur-CE composite. We also analyze the polysulfide solutions *via* UV–visible spectroscopy, and find that the solutions with CE and sulfur-CE samples, respectively, exhibit lower absorbance as compared to the blank (Fig. 6(c)). The further comparison of the UV–visible data obtained from the CE and sulfur-CE composite shows the pristine CE's excellent polysulfide-trapping capability. The sulfur-CE composite shows its capability to retain the high content of active material in the composite and further trap additional polysulfide. These results demonstrate the strong polysulfide-trapping capability of the CE and sulfur-CE; besides, the results of both cases would support the high-loading sulfur-CE cathode simultaneously with the high-loading capability and excellent electrochemical stability.

For a clearer understanding of the bonding environment in the CE and sulfur-CE, we examine the characteristic peaks of the C1s, O1s, and S2p X-ray photoelectron spectroscopy (XPS) spectra in Fig. 7. The C1s spectrum of CE, sulfur-CE, and the cycled sulfur-CE cathode after 200 cycles at a C/10 rate (Fig. 7(a)) reveals the main component framework in CE, which consists of various bonds, including C–C and C═C [46], C–O [47], C–O–C [46], C═O [46], and O–C═O [48]. These characteristic peaks in the C1s spectrum are consistent with the benzene, ether, and carbonyl groups in CE. Additionally, the C1s spectrum confirms that sulfur does not form specific bonding with carbon in CE during the sulfur-melting process. From the O1s spectrum of CE, sulfur-CE, and cycled sulfur-CE cathode (Fig. 7(b)), they all display two characteristic peaks for the C═O and the C–O–C functional groups [49]. After cycling, the cycled sulfur-CE cathode exhibits another peak indicative of the S–O bond [49], suggesting the chemisorption of polysulfides by the carbonyl groups of the CE substrate. Finally, the S2p spectrum of pure sulfur and sulfur-CE mainly features the elemental sulfur peaks of $2p_{3/2}$ and $2p_{1/2}$ [50], reconfirming that there is no chemical bonding formed during the incorporation of sulfur with CE (Fig. 7(c)). However, the cycled sulfur-CE cathode shows the characteristic peaks of the terminal ($S_T^{-1}$, 161.6 eV) and bridging sulfur ($S_B^0$, 163.3 eV) of the polysulfide and a little deposition of $Li_2S$ detected at 160.0 eV [49], which demonstrate the strong polysulfide adsorption. Some peaks in the region of 165 eV–171 eV correspond to the side products, thiosulfate (167.0 eV) [51] and sulfate (169.1 eV and 170.6 eV) [52]. Notably, we observe no peaks from the electrolyte solution, which may suggest the low electrolyte consumption in the cycled sulfur-CE cathode.

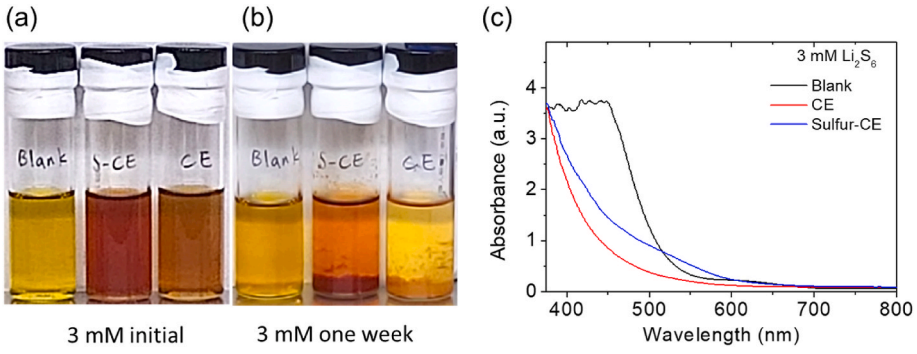


**Fig. 6.** The polysulfide adsorption test: the solution color of the polysulfide solutions without additives (labeled as blank), with sulfur-CE (labeled as S-CE), and with CE (labeled as CE), (a) before and (b) after static polysulfide adsorption for one week, and (c) the UV–visible analysis of the retrieved solutions after the static polysulfide adsorption. (For interpretation of the references to color in this figure legend, the reader is referred to the Web version of this article.)

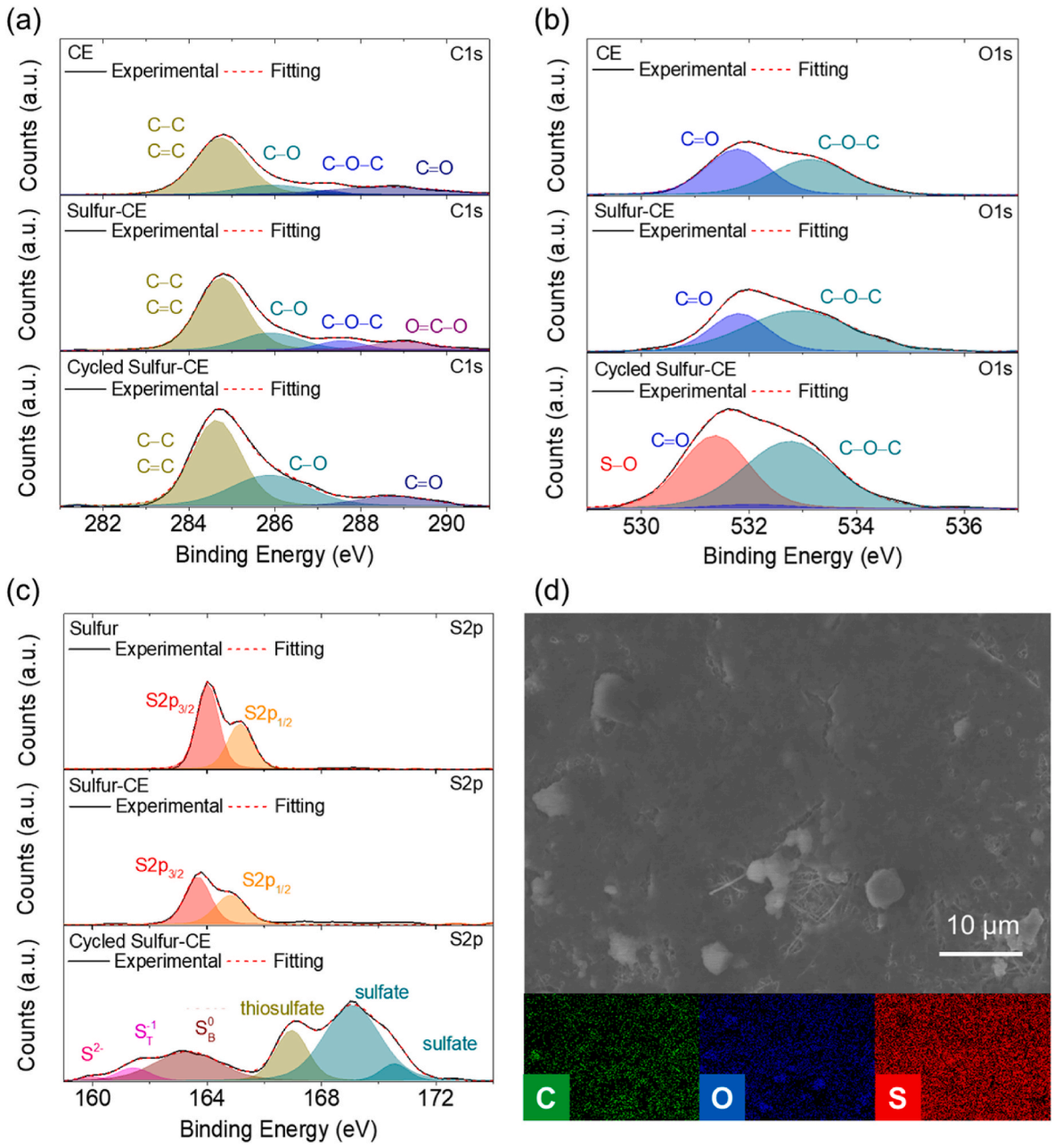


**Fig. 7.** The XPS analysis of sulfur, CE, sulfur-CE, and the cycled sulfur-CE cathode, including (a) the C1s spectrum, (b) the O1s spectrum, and (c) the S2p spectrum. (d) The SEM/EDS result of the cycled sulfur-CE cathode after 200 cycles, revealing the surface morphology and C, O, and S elemental distribution.

To further confirm the low electrolyte consumption of the CE as a sulfur host, we examine the cycling performance and the corresponding charge/discharge curves of the sulfur-CE cathode with electrolyte-to-sulfur ratios of 6, 8, and 10 μL $mg^{-1}$, as shown in Fig. S12. As compared to the cell with 4 μL $mg^{-1}$, these cells with the relatively sufficient amount of electrolyte show no initial activation process, while showing the same good cycle stability. As the electrolyte-to-sulfur ratio decreases from 10 to 6 μL $mg^{-1}$, the sulfur-CE cathode displays a similar stable cycling performance at a C/10 rate, with no significant drop of the charge-storage capacity for the lower electrolyte-to-sulfur ratio of 6 μL $mg^{-1}$. Moreover, there is no obviously increased polarization in 200 cycles as the amount of electrolyte decreases, indicating the cycling performance of the sulfur-CE cathode is not strongly affected. These results suggest that the CE as a sulfur host features low electrolyte consumption and benefits outstanding electrochemical stability at a low electrolyte-to-sulfur ratio, which demonstrates the great potential in the development of lean-electrolyte lithium-sulfur cells [1–3,53–56].

Based on the results of the polysulfide adsorption experiment, XPS analysis, and cycling performance with an electrolyte-to-sulfur ratio of 4 μL $mg^{-1}$, the strong retention of polysulfides in the cathode and electrolyte in electrochemical cell might be the key factor behind the device's stable long-term cyclability. Thus, the cycled high-loading sulfur-CE cathode is retrieved from the lean-electrolyte cell after 200 cycles (Fig. 7(d)), with a high-resolution SEM image in Fig. S13. The cycled sulfur-CE cathode still maintains the similar muddy surface and the strong elemental sulfur signal. These microstructural and elemental characteristics confirm that the smooth electrolyte environment and high amounts of polysulfide are both retained in the sulfur-CE cells, which affirms the importance of moderately high porosity of CE: it is porous enough to chemically adsorb polysulfide, but not porous enough to consume large amounts of electrolyte.

## 4. Conclusion

In this study, we investigate the incorporation of sulfur and CE as the sulfur-CE energy storage material. CE, as one of the PMCs, features perpendicular benzene walls that form a porous channel-like structure, and abundant carbonyl groups with polarity that provides active sites for the chemisorption of polysulfides. Thus, the sulfur-CE cathode is characterized by a high affinity to polysulfides, and maintains excellent electrochemical reactions without absorbing too much electrolyte. The sulfur-CE cathode features a high sulfur loading of 4 mg $cm^{-2}$ and a high sulfur content of 80 wt% with the lowest electrolyte-to-sulfur ratio of 4 μL $mg^{-1}$. This excellent cell design exhibits remarkable electrochemical performance with an outstanding charge-storage capacity of 907 mA h $g^{-1}$, high areal capacity and gravimetric capacity of 3.6 mA h $cm^{-2}$ and 726 mA h $g^{-1}$, respectively, a high rate performance of C/20–1C, and a long cycle life of 200 cycles at various cycling rates. These results suggest the strong potential of using PMCs to selectively trap polysulfides without absorbing excess electrolyte, which satisfies the two main requirements for high energy density lithium-sulfur cells: high-loading sulfur cathodes and lean-electrolyte cells.

## CRediT authorship contribution statement

**Yin-Ju Yen:** Conceptualization, Methodology, Investigation, Writing – original draft, preparation. **Teng-Hao Chen:** Conceptualization, Methodology, Writing – review & editing. **Yao-Ting Wang:** Resources. **Alexandra Robles:** Resources. **Miloš Đerić:** Resources. **Ognjen Š. Miljanić:** Resources, Methodology, Writing – review & editing. **Watchareeya Kaveevivitchai:** Conceptualization, Methodology, Writing – review & editing. **Sheng-Heng Chung:** Conceptualization, Methodology, Investigation, Writing – original draft, preparation, Writing – review & editing.

## Declaration of competing interest

The authors declare that they have no known competing financial interests or personal relationships that could have appeared to influence the work reported in this paper.

## Data availability

Data will be made available on request.

## Acknowledgements

This work is supported by the Ministry of Education (MOE) in Taiwan under Yushan Young Scholar Program and the National Science and Technology Council (NSTC) in Taiwan under grant 111-2636-E-006-027 (to S.-H. C.), 110-2113-M-006-011 (to T.-H. C.) and the Young Scholar Fellowship Program 110-2636-E-006-019 (to W. K.). This work was also financially supported by the Hierarchical Green-Energy Materials (Hi-GEM) Research Center, from the Featured Areas Research Center Program within the framework of the Higher Education Sprout Project by MOE to the Headquarters of University Advancement at National Cheng Kung University (NCKU). We acknowledge the use of XRD005101, EM000800, and ESCA000200 of MOST 111-2731-M-006-001 belonging to the Core Facility Center of National Cheng Kung University. We also acknowledge the support from the US National Science Foundation (award DMR-1904998 to O. Š. M.).

## Appendix A. Supplementary data

Supplementary data to this article can be found online at https://doi.org/10.1016/j.jpowsour.2023.232891.

## References

[1] M. Zhao, B.Q. Li, H.J. Peng, H. Yuan, J.Y. Wei, J.Q. Huang, Angew. Chem. Int. Ed. 59 (2020), 12636.
[2] J. He, A. Manthiram, Energy Storage Mater. 20 (2019) 55.
[3] G. Li, S. Wang, Y. Zhang, M. Li, Z. Chen, J. Lu, Adv. Mater. 30 (2018), 1705590.
[4] H.J. Peng, J.Q. Huang, X.B. Cheng, Q. Zhang, Adv. Energy Mater. 7 (2017), 1700260.
[5] R. Mukkabla, M.R. Buchmeiser, J. Mater. Chem. 8 (2020) 5379.
[6] X. Zhang, K. Chen, Z. Sun, G. Hu, R. Xiao, H.M. Cheng, F. Li, Energy Environ. Sci. 13 (2020) 1076.
[7] L. Huang, J. Li, B. Liu, Y. Li, S. Shen, S. Deng, C. Lu, W. Zhang, Y. Xia, G. Pan, X. Wang, Q. Xiong, Q. Xia, J. Tu, Adv. Funct. Mater. 30 (2020), 1910375.
[8] R. Fang, S. Zhao, S. Pei, X. Qian, P.X. Hou, H.M. Cheng, C. Liu, F. Li, ACS Nano 10 (2016) 8676.
[9] S.-H. Chung, A. Manthiram, ACS Appl. Mater. Interfaces 10 (2018), 43749.
[10] M. Wang, X. Xia, Y. Zhong, J. Wu, R. Xu, Z. Yao, D. Wang, W. Tang, X. Wang, J. Tu, Chem. Eur J. 25 (2019) 3710.
[11] L. Du, X. Cheng, F. Gao, Y. Li, Y. Bu, Z. Zhang, Q. Wu, L. Yang, X. Wang, Z. Hu, Chem. Commun. 55 (2019) 6365.
[12] X. Li, Y. Zhang, S. Wang, Y. Liu, Y. Ding, G. He, X. Jiang, W. Xiao, G. Yu, Nano Lett. 20 (2020) 6922.
[13] D.-R. Deng, X.-Y. Cui, X.-X. Fan, J.-Q. Zheng, X.-H. Fan, Q.-H. Wu, M.-S. Zheng, Q.-F. Dong, Sustain. Energy Fuels 5 (2021) 4284.
[14] S. Li, J. Lin, Y. Ding, P. Xu, X. Guo, W. Xiong, D.-Y. Wu, Q. Dong, J. Chen, L. Zhang, ACS Nano 15 (2021), 13803.
[15] Y. Yi, W. Huang, X. Tian, B. Fang, Z. Wu, S. Zheng, M. Li, H. Ma, ACS Appl. Mater. Interfaces 13 (2021), 59983.
[16] H. Liu, J. Wang, M. Sun, Y. Wang, R. Zhao, X. Zhang, Y. Zhao, Nanotechnology 33 (2021), 085704.
[17] Y. Liang, M. Xia, Y. Zhao, D. Wang, Y. Li, Z. Sui, J. Xiao, Q. Chen, J. Colloid Interface Sci. 608 (2022) 652.
[18] M. Li, Y. Wang, S. Sun, Y. Yang, G. Gu, Z. Zhang, Chem. Eng. J. 429 (2022), 132254.
[19] M. Zhao, B.Q. Li, X.Q. Zhang, J.Q. Huang, Q. Zhang, ACS Cent. Sci. 6 (2020) 1095.
[20] R. Fang, S. Zhao, Z. Sun, D.W. Wang, H.M. Cheng, F. Li, Adv. Mater. 29 (2017), 1606823.
[21] B. Wang, R.B. Lin, Z. Zhang, S. Xiang, B. Chen, J. Am. Chem. Soc. 142 (2020), 14399.
[22] M. Mastalerz, Acc. Chem. Res. 51 (2018) 2411.
[23] T.-H. Chen, I. Popov, W. Kaveevivitchai, Y.C. Chuang, Y.S. Chen, O. Daugulis, A. J. Jacobson, O.Š. Miljanić, Nat. Commun. 5 (2014) 5131.
[24] R.B. Lin, Y. He, P. Li, H. Wang, W. Zhou, B. Chen, Chem. Soc. Rev. 48 (2019) 1362.
[25] Y.-T. Wang, C. McHale, X. Wang, C.K. Chang, Y.C. Chuang, W. Kaveevivitchai, O.Š. Miljanić, T.-H. Chen, Angew. Chem. Int. Ed. 60 (2021), 14931.
[26] X. Liu, X. Yang, H. Wang, I. Hisaki, K. Wang, J. Jiang, J. Mater. Chem. 10 (2022) 1808.
[27] H. Li, Y. Huang, Y. Zhang, X. Zhang, L. Zhao, W. Bao, X. Cai, K. Zhang, H. Zhao, B. Yi, L. Su, A.K. Cheetham, S. Jiang, J. Xie, Nano Lett. 22 (2022) 2030.
[28] Y.-T. Wang, S. Jalife, A. Robles, M. Đerić, J.I. Wu, W. Kaveevivitchai, O.Š. Miljanić, T.-H. Chen, ACS Appl. Nano Mater. 5 (2022), 14021.
[29] H. Duan, K. Li, M. Xie, J.M. Chen, H.-G. Zhou, X. Wu, G.-H. Ning, A.I. Cooper, D. Li, J. Am. Chem. Soc. 143 (2021), 19446.
[30] G. Li, X. Wang, M.H. Seo, M. Li, L. Ma, Y. Yuan, T. Wu, A. Yu, S. Wang, J. Lu, Z. Chen, Nat. Commun. 9 (2018) 705.
[31] H. Du, S. Li, H. Qu, B. Lu, X. Wang, J. Chai, H. Zhang, J. Ma, Z. Zhang, G. Cui, J. Membr. Sci. 550 (2018) 399.
[32] C.M. McHale, C.R. Stegemoller, M.I. Hashim, X. Wang, O.S. Miljanić, Cryst. Growth Des. 19 (2019) 562.
[33] J. Xu, D. Su, W. Zhang, W. Bao, G. Wang, J. Mater. Chem. 4 (2016), 17381.
[34] X. Yang, L. Zhang, F. Zhang, Y. Huang, Y. Chen, ACS Nano 8 (2014) 5208.
[35] Y. Yu, W. Hu, I. Chou, L. Jiang, Y. Wan, Y. Li, Y. Xin, X. Wang, Geofluids 2021 (2021), 6658711.
[36] Z.A. Ghazi, L. Zhu, H. Wang, A. Naeem, A.M. Khattak, B. Liang, N.A. Khan, Z. Wei, L. Li, Z. Tang, Adv. Energy Mater. 6 (2016), 1601250.
[37] A. Bhargav, J. He, A. Gupta, A. Manthiram, Joule 4 (2020) 285.
[38] P.P. Wang, C.Y. Xu, W.D. Li, L. Wang, L. Zhen, Electrochim. Acta 169 (2015) 440.
[39] Y.-J. Yen, S.-H. Chung, Chem. Commun. 57 (2021), 2009.
[40] S.B. Tang, M.O. Lai, L. Lu, Mater. Chem. Phys. 111 (2008) 149.
[41] Z.W. Zhang, H.J. Peng, M. Zhao, J.Q. Huang, Adv. Funct. Mater. 28 (2018), 1707536.
[42] C.-S. Cheng, S.-H. Chung, Batter. Supercaps 5 (2022), e202100323.
[43] Y.-J. Yen, S.-H. Chung, ACS Appl. Mater. Interfaces 13 (2021), 58712.
[44] J. Pu, Z. Shen, J. Zheng, W. Wu, C. Zhu, Q. Zhou, H. Zhang, F. Pan, Nano Energy 37 (2017) 7.
[45] Z. Wu, S. Chen, L. Wang, Q. Deng, Z. Zeng, J. Wang, S. Deng, Energy Storage Mater. 38 (2021) 381.
[46] O. Akhavan, M. Kalaee, Z.S. Alavi, S.M.A. Ghiasi, A. Esfandiar, Carbon 50 (2012) 3015.
[47] B. Gurzęda, T. Buchwald, M. Nocuń, A. Bąkowicz, P. Krawczyk, RSC Adv. 7 (2017), 19904.
[48] Z. Yang, Y. Dai, S. Wang, H. Cheng, J. Yu, RSC Adv. 5 (2015), 78017.
[49] L. Tao, Y. Yang, H. Wang, Y. Zheng, H. Hao, W. Song, J. Shi, M. Huang, D. Mitlin, Energy Storage Mater. 27 (2020) 212.
[50] Z. Wang, Y. Dong, H. Li, Z. Zhao, H.B. Wu, C. Hao, S. Liu, J. Qiu, X.W.D. Lou, Nat. Commun. 5 (2014) 5002.

[51] M.I. Nandasiri, L.E. Camacho-Forero, A.M. Schwarz, V. Shutthanandan, S. Thevuthasan, P.B. Balbuena, K.T. Mueller, V. Murugesan, Chem. Mater. 29 (2017) 4728.
[52] C. Luo, E. Hu, K.J. Gaskell, X. Fan, T. Gao, C. Cui, S. Ghose, X.-Q. Yang, C. Wang, Proc. Natl. Acad. Sci. U.S.A. 117 (2020), 14712.
[53] S. Lang, X. Feng, J. Seok, Y. Yang, M.R. Krumov, A.M. Villarino, M.A. Lowe, S.-H. Yu, H.D. Abruña, Curr. Opin. Electrochem. 25 (2021), 100652.
[54] W. Guo, D.-Y. Wang, Q. Chen, Y. Fu, Adv. Sci. 9 (2022), 2103989.
[55] D.-Y. Wang, W. Wang, F. Li, X. Li, W. Guo, Y. Fu, J. Energy Chem. 71 (2022) 572–579.
[56] Y. Jeoun, M.-S. Kim, S.-H. Lee, J.H. Um, Y.-E. Sung, S.-H. Yu, Chem. Eng. J. 450 (2022), 138209.